ÖHÜ Müh. Bilim. Derg. / OHU J. Eng. Sci.
ISSN: 2564-6605
doi: 10.28948/ngumuh.598092
Ömer Halisdemir Üniversitesi Mühendislik Bilimleri Dergisi, Cilt 8, Sayı 2, (2019), 1143-1152
Omer Halisdemir University Journal of Engineering Sciences, Volume 8, Issue 2, (2019), 1143-1152

Araştırma / Research

EFFECT OF SOLIDIFICATION RATE ON CORROSION RESISTANCE OF CAST Al-10Mg_2Si IN-SITU COMPOSITES

Huseyin ZENGIN[1] (ORCID: 0000-0001-7518-1625)*

[1]*Karabuk University, Department of Metallurgical and Materials Engineering, 78050, Karabuk, Turkey*

Geliş / Received: *27.11.2018*
Kabul / Accepted: *21.02.2019*

ABSTRACT

The hypoeutectic Al-10Mg_2Si (wt%) composites, also denoted as Al-6.3Mg-3.7Si (wt%) alloy, were cast in a steel step mould, in which different solidification rates were obtained. The microstructural characterizations were made by optical microscope and XRD. Corrosion performances were measured by immersion and electrochemical corrosion tests in 3.5% NaCl solution. Microstructure analysis showed that all the alloys consisted of α-Al, Chinese script type Mg_2Si and needle-like Al_5FeSi phases. Increasing solidification rate resulted in a remarkable refinement of Chinese script-like eutectic Mg_2Si phases. Corrosion tests revealed that increasing solidification rate improved the corrosion resistance of Al-10Mg_2Si composites due to the more uniform distribution of Mg_2Si phases and the stabilization of protective oxide films on the sample surface.

Keywords: Aluminum alloys, solidification, casting, microstructure, corrosion

DÖKÜM Al-10Mg_2Si İN-SİTÜ KOMPOZİTLERİN KOROZYON DİRENCİNE KATILAŞMA HIZININ ETKİSİ

ÖZ

Al-6.3Mg-3.7Si (ağ.%) alaşımı olarak da adlandırılan hipoötektik Al-10Mg2Si (ağ.%) kompozitleri, farklı katılaşma oranlarının elde edildiği bir kademeli çelik kalıba dökülmüştür. Mikroyapısal karakterizasyonlar optik mikroskop ve XRD ile yapılmıştır. Korozyon performansları %3.5 NaCl çözeltisinde daldırma ve elektrokimyasal korozyon testleri ile ölçülmüştür. Mikroyapı analizleri, tüm alaşımlarda α-Al, Çin yazısı şekilli Mg_2Si ve iğnemsi Al_5FeSi fazlarının oluştuğunu göstermiştir. Katılaşma hızındaki artış, Çin yazısı şekilli ötektik Mg_2Si fazlarının önemli derece küçülmesine neden olmuştur. Korozyon testleri sonucunda artan katılaşma hızının Al-10Mg_2Si kompozitlerinin korozyon direncini arttırdığı görülmüştür ve bu da Mg_2Si fazlarının daha düzgün dağılımı ve numune yüzeyindeki koruyucu oksit filmlerinin daha kararlı hale gelmesi ile meydana gelmiştir.

Anahtar kelimeler: Alüminyum alaşımları, katılaşma, döküm, mikroyapı, korozyon

1. INTRODUCTION

Over the past few decades, cast aluminum alloys have attracted special attention mainly in automotive industry because of their high strength, low density and good castability compared to steel counterparts [1,2]. However, there is still need for improving their mechanical and corrosion properties to make them applicable for high performance materials. Regarding this, Al-Mg_2Si in-situ composites can be considered as a potential material since

*Corresponding author / Sorumlu yazar. Tel.: +90370 4187050; e-mail / e-posta: huseyinzengin@karabuk.edu.tr

they possess high melting temperature, high strength at elevated temperature and low thermal expansion [3]. Mg_2Si intermetallic compounds as the reinforcing material in Al matrix are the main reason for the improvement of properties and their size, distribution and morphology specify the final properties of the Al alloys. However, in hypereutectic Al-Mg_2Si composites, coarse and skeleton shaped Mg_2Si particles contain high stress concentration at their sharp edges and this leads to premature crack propagation and accordingly deteriorates mechanical properties [2,4]. Furthermore, the flake-like eutectic Mg_2Si particles cannot impede the crack propagation effectively either [5]. Among the Mg_2Si particles with different shapes, truncated octahedron crystals are more beneficial to mechanical properties [6]. Therefore, it is necessary to alter the size and distribution of Mg_2Si particles in order to make them beneficial. Recently, much efforts have been made on refinement of Mg_2Si compounds by mainly employment of different alloying elements such as Bi [7,8], Sb [9], Ce [2], Sr [10] and Gd [11]. Wu et al. showed that the morphology of the eutectic Mg_2Si phase transformed from plate-like structure to a thin coral-like and fibrous one by increasing Bi addition to Al-10Mg_2Si alloy [7]. Wang et al. reported that 0.5 wt% Sb addition changed the morphology of eutectic Mg_2Si phase from coarse dentrite to small polyhedral shape and significantly improved the mechanical properties of Al-20Mg_2Si-4Cu alloy [9]. Nordin et al. showed that after Ce addition, the skeleton Mg_2Si transformed to polygonal shape with decreased size and more uniform distribution and flake-like Mg_2Si phase changed to rod-like morphology [2]. It was also reported in the same study that the needle-like Al_5FeSi phase was refined by Ce addition. Furthermore, it was showed in another study that Sr addition resulted in a transformation of primary Mg_2Si phase from imperfect octahedron to polygonal morphology and also a transformation of eutectic Chinese script type Mg_2Si phase to fibrous and fish-bone morphology [10]. Ghandvar et al. showed that 1 wt% Gd addition altered the primary and eutectic Mg_2Si morphology from coarse dentritic and flake-like to truncated octahedral and rod-like shape, respectively [3,11]. Apart from this, it has been reported that different cooling conditions may result in a significant microstructural changes and thus mechanical properties [1,3,12]. Wang et al. [12] showed that increasing cooling rate led to a transformation of the morphology of primary Mg_2Si phase from perfect octahedron to truncated octahedron. However, there is no study in the literature about the effects of solidification rate on the microstructure of hypoeutectic Al-Mg_2Si in-situ composites. Furthermore, there is very limited study on the corrosion properties of Al-Mg_2Si in-situ composites and this study aims to clarify the relationship between the microstructural changes caused by different solidification rates and the corrosion properties of Al-Mg_2Si in-situ composites.

2. MATERIALS AND METHOD

Al-6.3Mg-3.7Si (wt%) alloy, corresponding to hypoeutectic Al-10Mg_2Si alloy, was prepared in an electrical resistance furnace by use of pure Al ingots (≥ 99 wt%), pure Mg ingots (≥ 99.5 wt%) and Al-30Si (wt%) master alloys. Firstly, Al ingots and Al-30Si master alloys were melted at 750 °C and Mg ingots (with an extra addition of 15% to compensate the oxidation loss) were added into the melt at this temperature. Subsequently, 0.5 wt% dry C_2Cl_6 degassing tablets were applied. After stirring for 10 min and cleaning off the slag, the melt was poured into a steel step mould preheated to 200 °C. As shown in Fig. 1, the stepped design contains different section thicknesses, which provides different cooling rates. The temperature of each section was simultaneously measured at their centre by K-type thermocouples connected to a data acquisition equipment. The thermocouples were already placed in the mould before pouring the melt. After the solidification, the thermocouples were cut off and the cast alloy was sectioned as illustrated in Fig. 1. The chemical composition of the alloy taken from section 2 was measured by wave-length dispersion X-ray fluorescence (XRF-Rigaku-ZSX Primus II) and the results are given in Table 1. Because the chemical composition results were in line with the alloy design, the casting process was not repeated.

Table 1. Chemical compositions of the studied alloy (wt%)

Alloy	Mg	Si	Fe	Mn	Cr	Ni	Ca	Al
Al-10Mg2Si	6.26	3.85	0.19	0.02	0.02	0.01	0.02	Bal.

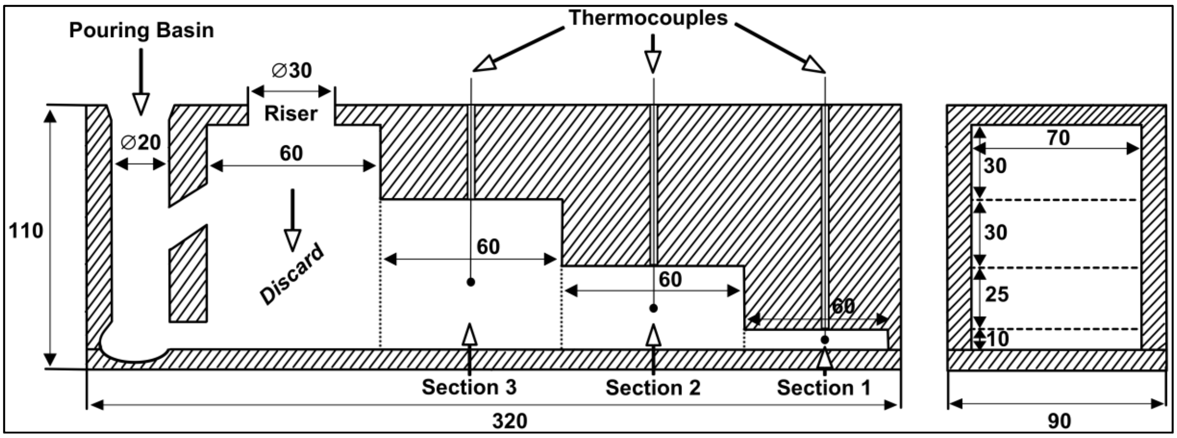

Figure 1. Schematic diagram of stepped design permanent mould

Metallographic samples were taken from near centre of each section and standard routine was used for mechanical grinding and polishing. After that, an etchant of 1 vol% HF in water solution was used for 20 s. Microstructures were taken by optical microscope (OM). The constituent phases were analysed by Rigaku Ultima IV X-ray diffractometer (XRD).

The constant immersion corrosion test specimens were cut from the near centre of each section as rectangular shape with the dimension of 20 mm x 10 mm x 2 mm. The samples were ground up to 2500 grid emery paper before the immersion tests. After that, the specimens were immersed in 3.5 wt% NaCl solution for 12 days at room temperature. The removal of corrosion products formed on the surface after the immersion tests was done by dipping in 50 vol% HNO_3 solution for 3 min. Then the weight loss measurements were made and corrosion rates were calculated. The cross sections of the corroded surfaces were analysed by OM. At least three specimens were used for the immersion tests for each section. The electrochemical corrosion tests were also carried out in 3.5 wt% NaCl solution. A classical three-electrode cell was used with a graphite rod as counter electrode, a saturated calomel electrode (SCE) as reference electrode and the sample as working electrode. Gamry model PC4/300 mA potentiostat was used for both potentiodynamic polarization and potentiostatic electrochemical impedance spectroscopy (EIS) tests. The polarization curves were obtained at a scan rate of 1 mVs-1, starting from -0.25 V (vs. E_{oc}) to +0.25 V (vs. E_{oc}). The corrosion current densities were calculated by Tafel extrapolation method. In the EIS tests, the frequency range was from 60 kHz to 0.4 Hz and the voltage amplitude was set to 20 mV. Both electrochemical tests were repeated at least three times to supply reproducibility.

3. RESULTS AND DISCUSSION

The cooling curves of the Al-10Mg_2Si composites simultaneously measured during solidification are presented in Fig. 2. It is evident that the cooling rate during solidification gradually decreased as stepping up in the steel mould, meaning that sections with larger thickness cooled more slowly. The average cooling rate can be estimated by [13]

$$V_{average} = \frac{(T_1 - T_2)}{\Delta t} \qquad \text{Eq. 1}$$

where $V_{average}$ is the average cooling rate, T_1 is the initial temperature, T_2 is the final temperature and Δt is the time passed between these temperatures. Here, the final temperature can be chosen as 500 °C. According to Eq. 1, the average cooling rates of the Al-10Mg_2Si composites calculated as 0.78, 0.33 and 0.17 °C/s at the sections of 1, 2 and 3, respectively.

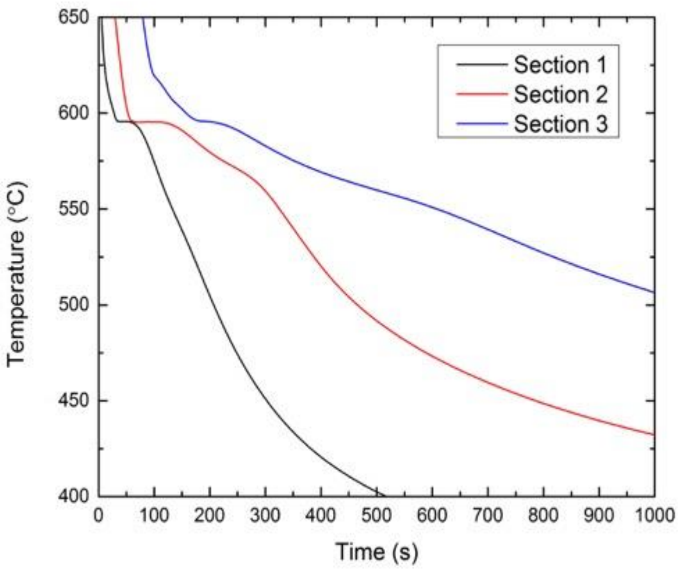

Figure 2. Cooling curves of the Al-10Mg_2Si alloys during casting and solidification

Fig. 3 shows the XRD patterns of the Al-10Mg_2Si alloy. Since different cooling rates did not lead to any formation of a new compound, only the XRD pattern taken from the Section 2 was presented in Fig. 3. It can be seen that the constituent phases consisted of α-Al, Mg_2Si and Al_5FeSi phases in the Al-10Mg_2Si alloy. From Fig. 4, the morphology and distribution the intermetallic phases can be seen clearly. According to Al-Mg_2Si phase diagram [14], α-Al + $Mg_2Si_{(eutectic)}$ phases form after the solidification of Al-10wt% Mg_2Si alloy. The eutectic Mg_2Si phases formed as the shape of Chinese script consisting of thin strips in a white α-Al matrix. Similar Chinese script-like morphology of Mg_2Si phases were observed in previous studies [3,7,8,15]. In Fig. 4, the microstructures of the sections having different cooling rates contained nearly same amount of second phases. However, the size of Chinese script-like eutectic Mg_2Si phases exhibited a remarkable refinement with increasing cooling rate. The specimen from Section 1 revealed more refined microstructure whereas the second phases were the largest in the microstructure taken from Section 3. The Al_5FeSi phases were identified in the microstructures based on its distinctive needle-like morphology as it has been reported in previous studies [2,16,17]. The Al_5FeSi usually form in the remaining solidified liquid when there is Fe in the Al-Si system even with small fraction [16]. This phase is very hard and brittle and does not have a strong bond with the Al matrix [18]. According to sludge factor (SF), which calculated as SF = 1 wt%Fe + 2 wt% Mn + 3 wt% Cr, a SF value below 2 will not give rise to sludge formation at a casting temperature of 650 °C and above [19]. In the present study, the SF factor was calculated as 0.3 according to Table 1, which is much lower than 2. Accordingly, no star-like or exploded sludge formation containing high amounts of Al, Si, Fe, Mn and Cr were observed as reported in previous studies for the alloys having SF factor mostly above 2 [18,19]. However, as outlined above, although no Fe addition was made in this study, the formation of Al_5FeSi phase was due to the Fe contamination caused by the impurity elements in the ingots used during casting. It is also worth noting that the length of needle-like Al_5FeSi phases increased with decreasing cooling rate as it can be seen in Fig. 4. It is because the growth of Al_5FeSi phase becomes difficult at faster cooling rates since the precipitation approaches the solidification onset of eutectic Al-Si [20]. Seifeddine et al. [21] showed that needle-like Al_5FeSi phase can form even at high cooling rates and high ratio of Mn to Fe. Therefore, the complete removal of these harmful precipitates is challenging.

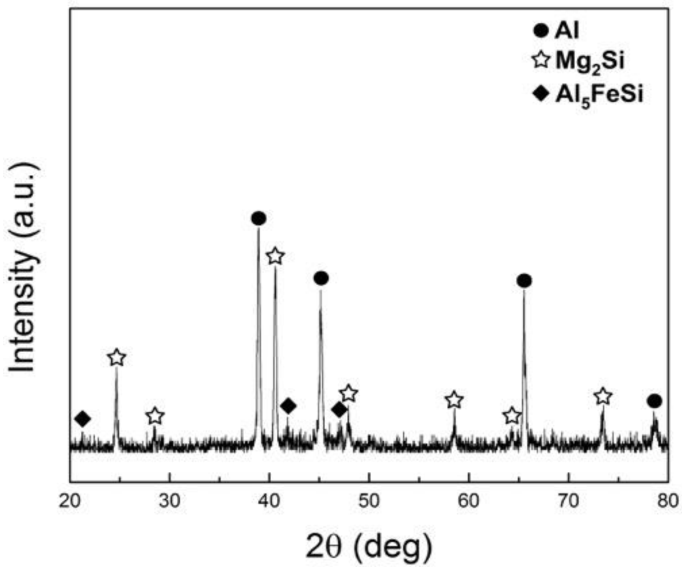

Figure 3. XRD pattern of the Al-10Mg_2Si alloys taken from Section 2

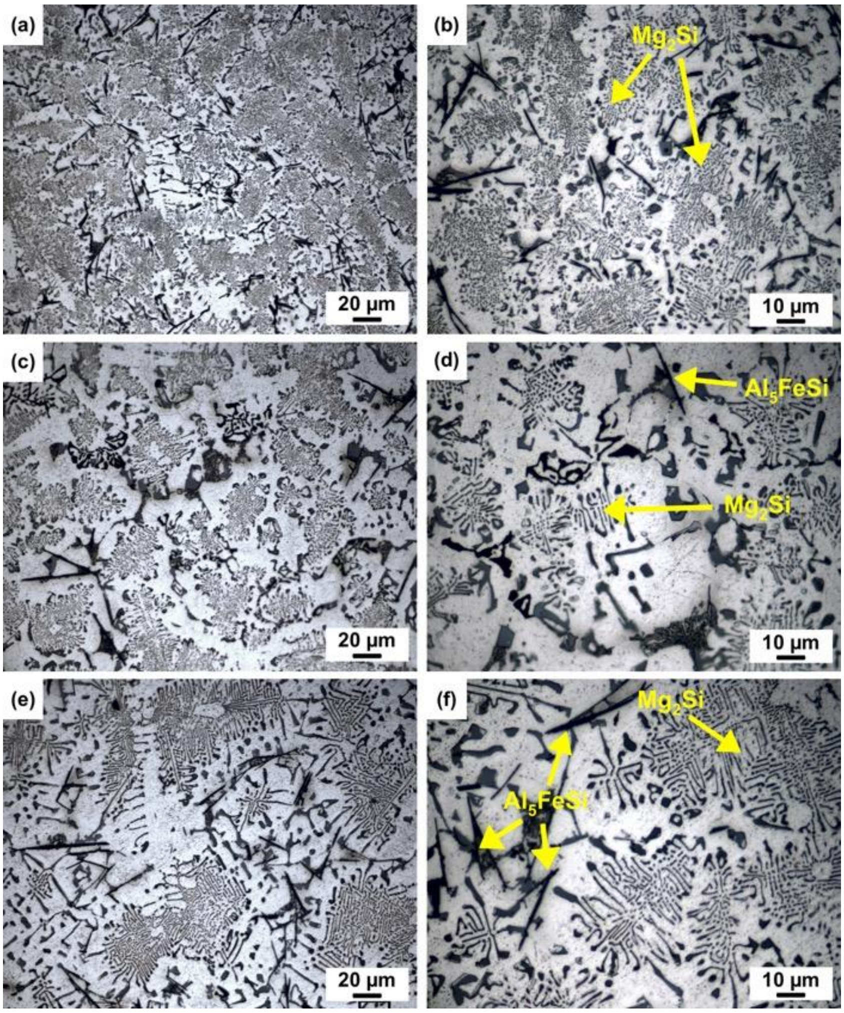

Figure 4. Microstructures of the Al-10Mg_2Si alloys with different magnifications taken from (a,b) Section 1, (c,d) Section 2 and (e,f) Section 3

The weight loss measurements obtained from the immersion tests at different days are presented in Fig. 5. The weight loss values increased gradually with increasing immersion time for all the sections. It seems that the corrosion resistance of Al-10Mg_2Si composite was drastically improved as the solidification rate increased. The alloy taken from Section 1 showed the best corrosion performance. The results of the potentiodynamic polarization tests are illustrated in Fig. 6. The results showed that the corrosion potential values (E_{corr}) did not show a considerable change. However, at the fastest cooling rate, the E_{corr} values were shifted toward to more noble value. Furthermore, it is agreed that higher corrosion current density values (i_{corr}) characterize higher corrosion rate [22]. In the present study, the i_{corr} values, obtained from the polarization curves in Fig. 6, were estimated as 4.78, 5.96 and 11.4 μA/cm^2 for Section 1, Section 2 and Section 3, respectively. Therefore, the corrosion rate decreased as the solidification rate increased, revealing that the results were in line with the immersion test results shown in Fig. 5.

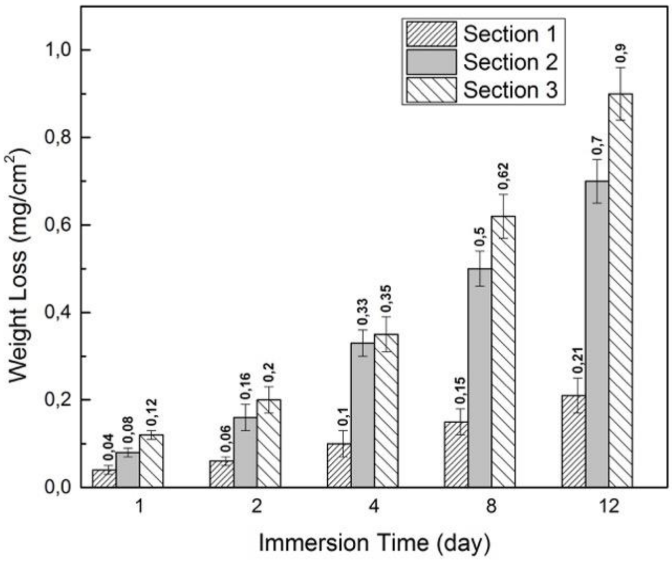

Figure 5. Immersion test results of the Al-10Mg_2Si alloys

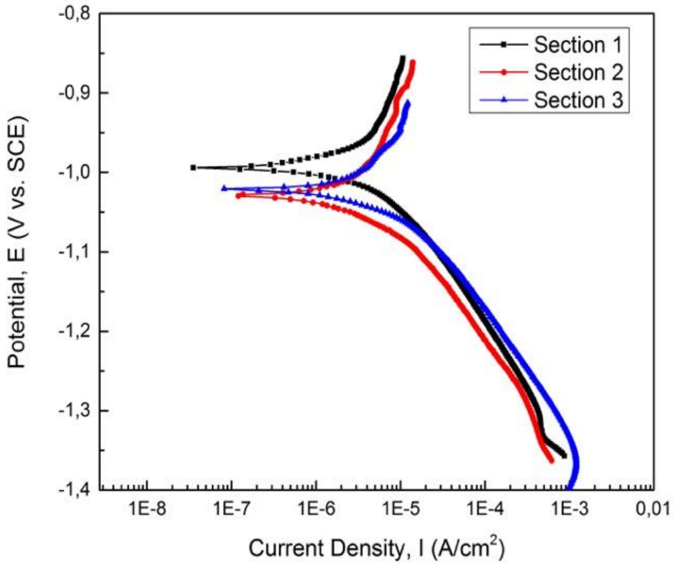

Figure 6. Potentiodynamic polarization curves of Al-10Mg_2Si alloys

The Nyquist plots of the studied alloys with corresponding equivalent circuit are demonstrated in Fig. 7. As it can be seen, all the EIS spectras exhibited one capacitive loop at medium frequencies. The only distinct difference among the EIS spectras seemed to be the diameters of the arcs, indicating that their corrosion rates were different based on the microstructural changes. Generally speaking, the larger medium frequency capacitive loop indicates an improvement of the corrosion resistance. In Fig. 7, the diameter of the capacitive loop for the Section 1 was the larger compared to other sections and it became smaller with decreasing solidification rate. This indicated that the higher solidification rate led to better corrosion resistance due to the stabilization of the protective oxide film on the surface [23]. Furthermore, the EIS test results were fitted in accordance with the equivalent circuit which illustrated as the inset in Fig. 7. In that equivalent circuit model, R_s, R_1 and R_2 represent solution resistance, corrosion product resistance at the sample surface and charge transfer resistance, respectively. CPE_1 and CPE_2 are the constant phase elements, which characterize the capacity of the oxide film and the electric double layer capacity at the interface of solution and sample. It is generally accepted that the R_1 and R_2 values have a direct proportional to corrosion resistance. The higher R_1 and R_2 values indicate more difficult charge transfer between the sample and solution [24,25]. The R_1 values of 473, 305 and 118 Ω/cm^2 and the R_2 values of 1623, 1014, 773 Ω/cm^2 were calculated for the alloys taken from Section 1, Section 2 and Section 3, respectively. It is evident that both resistance values showed a decrease as the solidification rate decreased, indicating that higher solidification rate induced more stable protective layer of oxide film and improved corrosion resistance. Ozturk et al. [26] also reported similar capacitive loops for A356 alloy with and without Sr additions and resistance of oxide layer value found the highest in Sr-modified samples, indicating a barrier effect caused by Sr addition.

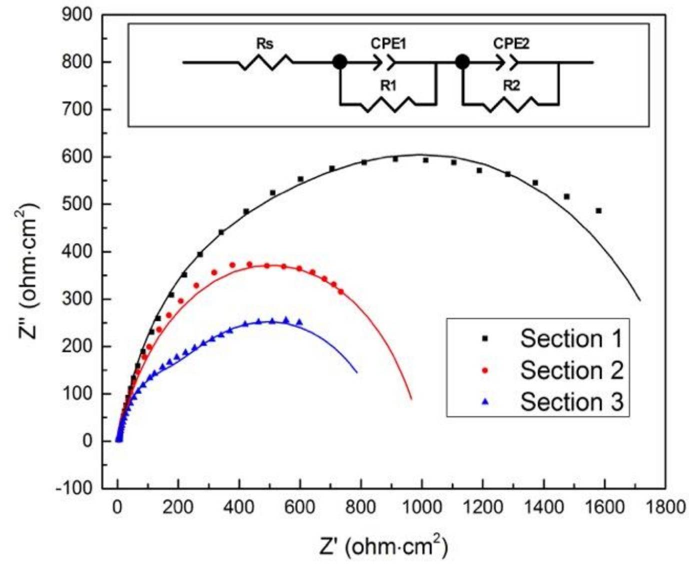

Figure 7. Nyquist plots with an inset graph showing the equivalent circuit of EIS spectra of Al-10Mg_2Si alloys

Both the immersion and electrochemical corrosion tests showed that higher cooling rates of Al-10Mg_2Si composites during solidification can improve the corrosion resistance. Since the alloys studied in this study have the same chemical composition but different solidification rates and thus different microstructural characteristics, the difference in the corrosion rates can be explained by only the microstructure differences among the alloys. As outlined earlier, higher solidification rate resulted in finer Chinese script type Mg_2Si intermetallics (see Fig. 4). Abdel Rehim et al. showed that the resistance of the protective film incresed and the pitting corrosion resistance was improved by Si addition to Al [27]. Additionally, the role of Mg_2Si intermetallics on corrosion resistance of Al alloys was investigated by Escalera-Lozano et al. and they reported that Mg_2Si tended to form MgO and SiO_2 oxides and these oxides protected Mg_2Si particles from microgalvanic corrosion with α-Al matrix [23]. They also reported that Al-Fe-Si containing intermetallics did not affect the corrosion resistance. However, Arrabal et al. [28] measured the surface potential maps of A356 alloy by Kelvin probe force microscopy and showed that Al-Fe-Si intermetallic had higher potentials than the α-Al, meaning that it was cathodic to α-Al matrix and Mg_2Si intermetallic exhibited more negative potential, indicating an anodic behavior with respect to α-Al. It was also reported in several studies that in Al-Mg_2Si composites, potential of Mg_2Si is negative to that of α-Al at the initial stage of corrosion and thus, corrosion initiates at Mg_2Si particles by dissolution of Mg and results in an enrichment of Si in these particles [29,30]. Eventually, Mg_2Si particles became cathode and led to formation of pits.

The SEM micrographs of the corroded surfaces after 12 h immersion tests are illustrated in Fig. 8. It can be seen that none of the studied alloys exhibited severe corrosion throughout the surface. Furthermore, it is also clear that α-Al matrix phase in the studied alloys showed very few dissolution whereas most of the dissolution occurred around second phase particles. As stated earlier, Al_5FeSi, having higher potentials than α-Al, always acted as cathode during the corrosion process and caused degradation around (dissimilar to Ref. [23]) it while the adverse effects of Mg_2Si phase on the corrosion propagation were seen as the corrosion proceeded as dissolution of matrix around the particles due to the polarity conversion between Mg_2Si and α-Al. Since the size of Al_5FeSi phase in the alloy Section 1 was much smaller than that in the other sections, the alloy Section 1 exhibited lower weight loss and better corrosion resistance.

Therefore, the corrosion improvement by increased solidification rate in this study can be attributed to the following aspects. Firstly, the formation of more stable oxide films and accordingly protection of microgalvanic coupling of Al_5FeSi and Mg_2Si particles with α-Al matrix. The finer Chinese script type Mg_2Si consisting of tiny Mg_2Si particles with larger surface area and their uniform distribution likely resulted in formation of more MgO and SiO_2 oxides and stabilized the protective surface film. Secondly, the finer Al_5FeSi phases at higher cooling rates resulted in less localized corrosion attack since they can act as local cathodic sites during the corrosion process because of their higher potential compared to α-Al [28,30]. Accordingly, the refinement of Chinese script type Mg_2Si and needle-like Al_5FeSi phases can play a beneficial role on the corrosion protection of Al-Mg_2Si in-situ composites from further attack in NaCl solution.

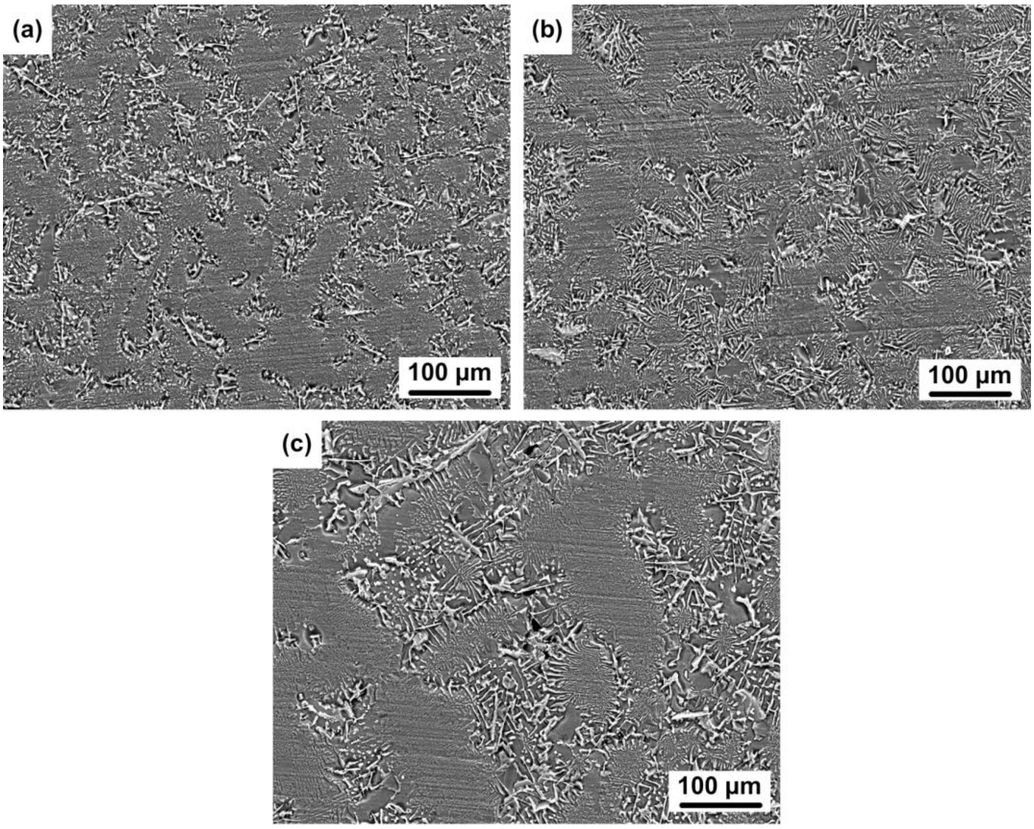

Figure 8. SEM micrographs of the corroded surfaces after 12 h immersion in 3.5 % NaCl solution after removal of corrosion product: (a) Section 1, (b) Section 2 and (c) Section 3.

4. CONCLUSION

Al-10Mg_2Si alloys were successfully cast in a steel step mould to provide different solidification rates. The corrosion resistances were measured by immersion and electrochemical tests and following conclusions were drawn:

- The constituent phases consisted of α-Al, Mg_2Si and Al_5FeSi phases in the Al-10Mg_2Si alloys.
- The eutectic Mg_2Si phases formed as the shape of Chinese script consisting of thin strips in a white α-Al matrix.
- The Chinese script-like eutectic Mg_2Si phases exhibited a remarkable refinement with increasing cooling rate.

- Both the immersion and electrochemical corrosion tests showed that increasing solidification rate improved the corrosion resistance of Al-10Mg$_2$Si composites.
- The corrosion improvement by increased solidification rate was attributed to the formation of more stable oxide films and accordingly protection of microgalvanic coupling of Mg$_2$Si particles with α-Al matrix caused by more uniform distribution of tiny Mg$_2$Si particles with larger surface area and decreased local cathodic effects of needle-like Al$_5$FeSi phases with increasing solidification rate.

REFERENCES

[1] OKAYASU, M., YOSHIDA, S., "Influence of solidification rate on material properties of cast aluminium alloys based on Al–Si–Cu and Al–Si–Mg", International Journal of Cast Metals Research, 28, 105–116, 2015.

[2] NORDIN, N.A., FARAHANY, S., ABU BAKAR, T.A., HAMZAH, E., OURDJINI, A., "Microstructure development, phase reaction characteristics and mechanical properties of a commercial Al–20%Mg2Si–xCe in situ composite solidified at a slow cooling rate", Journal of Alloys and Compounds, 650, 821–834, 2015.

[3] GHANDVAR, H., IDRIS, M.H., AHMAD, N., EMAMY, M., "Effect of gadolinium addition on microstructural evolution and solidification characteristics of Al-15%Mg2Si in-situ composite", Materials Characterization, 135, 57–70, 2018.

[4] NORDIN, N.A., FARAHANY, S., OURDJINI, A., ABU BAKAR, T.A., HAMZAH, E., "Refinement of Mg2Si reinforcement in a commercial Al–20%Mg2Si in-situ composite with bismuth, antimony and strontium", Materials Characterization, 86, 97–107, 2013.

[5] ZHANG, J., FAN, Z., WANG, Y., ZHOU, B., "Microstructural refinement in Al–Mg2Si in situ composites", Journal of Materials Science Letters, 18, 783–784, 1999.

[6] CHEN, L., WANG, H.Y., LI, Y.J., ZHA, M., JIANG, Q.C., "Morphology and size control of octahedral and cubic primary Mg2Si in an Mg–Si system by regulating Sr contents", CrystEngComm, 16, 448–454, 2013.

[7] WU, X.-F., WANG, Y., WANG, K.-Y., ZHAO, R.-D., WU, F.-F.," "Enhanced mechanical properties of hypoeutectic Al-10Mg2Si cast alloys by Bi addition", Journal of Alloys and Compounds, 767, 163–172, 2018.

[8] GUO, E.J., MA, B.X., WANG, L.P., "Modification of Mg2Si morphology in Mg–Si alloys with Bi", Journal of Materials Processing Technology, 206, 161–166, 2008.

[9] WANG, H., LIU, F., CHEN, L., ZHA, M., LIU, G., JIANG, Q., "The effect of Sb addition on microstructures and tensile properties of extruded Al–20Mg2Si–4Cu alloy", Materials Science and Engineering: A, 657, 331–338, 2016.

[10] JIANG, W., XU, X., ZHAO, Y., WANG, Z., WU, C., PAN, D., MENG, Z., "Effect of the addition of Sr modifier in different conditions on microstructure and mechanical properties of T6 treated Al-Mg2Si in-situ composite", Materials Science and Engineering: A, 721, 263–273, 2018.

[11] GHANDVAR, H., IDRIS, M.H., AHMAD, N., "Effect of hot extrusion on microstructural evolution and tensile properties of Al-15%Mg2Si-xGd in-situ composites", Journal of Alloys and Compounds, 751, 370–390, 2018.

[12] WANG, D., ZHANG, H., GUO, C., WU, H., CUI, J., "Effect of cooling rate on growth and transformation of primary Mg2Si in Al–Mg2Si in situ composites", Journal of Materials Research, 1–8, 2018.

[13] XU, C.L., WANG, H.Y., QIU, F., YANG, Y.F., JIANG, Q.C., "Cooling rate and microstructure of rapidly solidified Al–20wt.% Si alloy", Materials Science and Engineering: A, 417, 275–280, 2006.

[14] LI, S., ZHAO, S., PAN, M., ZHAO, D., CHEN, X., BARABASH, O.M., BARABASH, R.I., "Solidification and Structural Characteristics of α(Al)–Mg2Si Eutectic", Materials Transactions, 38, 553–559, 1997.

[15] AHLATCI, H., "Production and corrosion behaviours of the Al–12Si–XMg alloys containing in situ Mg2Si particles", Journal of Alloys and Compounds, 503, 122–126, 2010.

[16] FARAHANY, S., NORDIN, N.A., OURDJINI, A., ABU BAKAR, T., HAMZAH, E., IDRIS, M.H., HEKMAT-ARDAKAN, A., "The sequence of intermetallic formation and solidification pathway of an Al–13Mg–7Si–2Cu in-situ composite", Materials Characterization, 98, 119–129, 2014.

[17] KARANTZALIS, A.E., LEKATOU, A., GEORGATIS, E., POULAS, V., MAVROS, H., "Microstructural Observations in a Cast Al-Si-Cu/TiC Composite", Journal of Materials Engineering and Performance, 19, 585–590, 2010.

[18] SHABESTARI, S.G., "The effect of iron and manganese on the formation of intermetallic compounds in aluminum–silicon alloys", Materials Science and Engineering: A, 383, 289–298, 2004.

[19] MAKHLOUF, M.M., APELIAN, D., "Casting Characteristics of Aluminum Die Casting Alloys", Worcester Polytechnic Institute (US), 2002.

[20] BELMARES-PERALES, S., CASTRO-ROMÁN, M., HERRERA-TREJO, M., RAMÍREZ-VIDAURRI, L.E., "Effect of cooling rate and Fe/Mn weight ratio on volume fractions of α-AlFeSi and β-AlFeSi phases in Al−7.3Si−3.5Cu alloy", Metals and Materials International, 14, 307–314, 2008.

[21] SEIFEDDINE, S., JOHANSSON, S., SVENSSON, I.L., "The influence of cooling rate and manganese content on the β-Al5FeSi phase formation and mechanical properties of Al–Si-based alloys", Materials Science and Engineering: A, 490, 385–390, 2008.

[22] ZENGIN, H., TUREN, Y., AHLATCI, H., SUN, Y., "Mechanical Properties and Corrosion Behavior of As-Cast Mg-Zn-Zr-(La) Magnesium Alloys", Journal of Materials Engineering and Performance, 27, 389–397, 2018.

[23] ESCALERA-LOZAN, R., PECH-CANUL, M.I., PECH-CANUL, M.A., MONTOYA-DÁVILA, M., URIBE-SALAS, A., "The Role of Mg2Si in the Corrosion Behavior of Al-Si-Mg Alloys for Pressureless Infiltration", The Open Corrosion Journal, 3, 2010.

[24] SRINIVASAN, A., NINGSHEN, S., KAMACHI MUDALI, U., PILLAI, U.T.S., PAI, B.C., "Influence of Si and Sb additions on the corrosion behavior of AZ91 magnesium alloy", Intermetallics, 15, 1511–1517, 2007.

[25] KHARITONOV, D.S., DOBRYDEN, I.B., SEFER, B., ZHARSKII, I.M., CLAESSON, P.M., KURILO, I.I., "Corrosion of AD31 (AA6063) Alloy in Chloride-Containing Solutions", Protection of Metals and Physical Chemistry of Surfaces, 54, 291–300, 2018

[26] ÖZTÜRK, İ., HAPÇI AĞAOĞLU, G., ERZI, E., DISPINAR, D., ORHAN, G., "Effects of strontium addition on the microstructure and corrosion behavior of A356 aluminum alloy", Journal of Alloys and Compounds, 763, 384–391, 2018.

[27] ABDEL REHIM, S.S., HASSAN, H.H., AMIN, M.A., "Chronoamperometric studies of pitting corrosion of Al and (Al–Si) alloys by halide ions in neutral sulphate solutions", Corrosion Science, 46, 1921–1938, 2004.

[28] ARRABAL, R., MINGO, B., PARDO, A., MOHEDANO, M., MATYKINA, E., RODRÍGUEZ, I., "Pitting corrosion of rheocast A356 aluminium alloy in 3.5wt.% NaCl solution", Corrosion Science, 73, 342–355, 2013.

[29] LI, Z., LI, C., GAO, Z., LIU, Y., LIU, X., GUO, Q., YU, L., LI, H., "Corrosion behavior of Al–Mg2Si alloys with/without addition of Al–P master alloy", Materials Characterization, 110, 170–174, 2015. doi:10.1016/j.matchar.2015.10.028.

[30] ZENG, F., WEI, Z., LI, J., LI, C., TAN, X., ZHANG, Z., ZHENG Z., "Corrosion mechanism associated with Mg2Si and Si particles in Al–Mg–Si alloys", Transactions of Nonferrous Metals Society of China, 21, 2559–2567, 2011.